Effect of Bismuth Oxide Particles Size on the Thermal Excitation and Combustion Properties of Thermite Systems

Shi Li, Tao Guo,* Miao Yao, Jiaxing Song, Wen Ding, Yiming Mao,* and Jialin Chen[a]

The influence of Bi_2O_3 particles size at the sub-micron scale on the thermal excitation threshold and combustion performance of nano-thermite systems was investigated. Three formulas were designed and prepared, Al(100 nm)/Bi_2O_3(170 nm), Al-(100 nm)/Bi_2O_3(370 nm) and Al(100 nm)/Bi_2O_3(740 nm). The samples were characterized and tested by SEM, XRD, and DSC techniques. Electrical ignition and combustion experiments were performed. The results showed that with the increase of the particle size of Bi_2O_3, in the case of slow linear heating, the exothermic heat decreased (1051.2 $J g^{-1}$, 527.3 $J g^{-1}$ and 243.6 $J g^{-1}$) and the thermal excitation threshold temperature increased (564.52 °C, 658.1 °C and 810.9 °C). Simultaneously, the state of the thermite reaction correspondingly changed to solid-solid, liquid-solid and liquid-liquid thermite reaction. In the case of rapid heating , the increase in particle size increased the excitation current (0.561A, 0.710A and 0.837A). During the combustion process, the thermite system with the smallest Bi_2O_3 particle size showed the largest combustion rate, and that with the largest particle size had the longest combustion duration.

1. Introduction

Metal fuels represented by Al powder have attracted widespread attention due to their high volumetric energy, wide sources, and economical price.[1,2] The mixture of nano-Al powder and oxidant assembled by physical blending, electrostatic spraying or chemical coating is called nano-thermite.[3–5] Under certain excitation conditions, it can undergo violent oxidation-reduction reactions and emit a large amount of heat.[6,7] The excellent performance of nano-thermite makes it shine in the fields of micro explosion,[8] railway welding,[9,10] solid propellant,[11–13] and pyrotechnic agent.[14]

The combustion performance of the thermite depends largely on the particle size distribution of the components. The smaller the particle size, the more contact points between the metal fuel and the oxide, which will change the performance of the thermite.[15] At present, many studies have explored the influence of Al powder particle size on the thermite system. L. Wang et al. studied the effect of Al particle size on the pressure pulse release rate of the nano-thermite reaction in the Bi_2O_3/Al system. The results showed that the pressure pulse release rate of the nano-thermite reaction was much greater than that of the micron-sized thermite agent.[16] Sang Beom Kim et al. studied the combustion and gas generation properties of NaN_3-Al-CuO systems with different Al powder particle sizes. The results showed that nano-Al powder exhibits more excellent reactivity, and higher exothermic performance and gas production performance.[17]

The reduction in the particle size of the Al powder has greatly improved the thermite's combustion rate, gas production, and heat release performance. However, due to the oxidation of the Al powder surface, the active Al content of Al powders with a diameter of less than 35 nm is low. It is not beneficial to the improvement of performance but plays a hindrance.[18] Therefore, research on the influence of oxide particle size on the combustion performance of the thermite system has gradually emerged. M.R. Weismiller et al. studied the influence of the particle size of fuel and oxidant between nanometer and micrometer on the propagation rate and reaction temperature. The results showed that the mixture containing nano-sized oxidant particles had a shorter heating time and a shorter gas diffusion length scale than micro-sized particles.[19] In the study of Garth C. Egan et al., the pressure generated by the combustion of Al/nano-CuO thermite was five times that of Al/micro-CuO.[20] The previous study only compare the performance of nano-thermite and micro-thermite, but do not study the specific performance change of oxide particle size in the range of 100 nm–1 um.[19–21]

Traditional oxidants are composed of Fe_2O_3, CuO, MnO_2, etc. These oxidants have good thermal properties but relatively low gas production.[22] Compared with these oxidants, Bi_2O_3 has the characteristics of high energy release rate and high gas production.[23] At the same time, due to the low melting point of bismuth, the mixture of Bi_2O_3 and Al powder will release a large amount of gas[16] during the combustion process. It has shown excellent effects in the detonator,[24] rocket propellant,[25] etc. V. Eric Sanders et al. used unconfined and closed combustion experiments to quantitatively analyze the reaction performance of Al/Bi_2O_3 nano-thermite through pressure output and propagation velocity.[26]

[a] Dr. S. Li, Dr. T. Guo, Dr. M. Yao, Dr. J. Song, Dr. W. Ding, Dr. Y. Mao, Dr. J. Chen
College of Field Engineering
Army Engineering University of PLA
Nanjing, 210007 (China)
E-mail: 2636594092@qq.com
guotao3579@126.com

In this paper, on the basis of previous studies, Bi_2O_3 with different particle sizes were prepared by hydrothermal method. Al and Bi_2O_3 powder were mixed and dispersed by ultrasonic to obtain thermite sample. The morphology, purities were characterized by SEM and XRD. Through DSC, electric ignition test and high-speed photography, the thermal properties and combustion properties of the products were studied. The effect of Bi_2O_3 particle size on the overall properties of aluminothermic system was understood more clearly.

2. Results and Discussion

2.1. Purity and Morphology Analysis of Bi_2O_3

The morphology, particle size and purity of self-made Bi_2O_3 samples were detected.

Figure 1 shows the FE-SEM images of the synthesized Bi_2O_3 and its particle size distribution. Figure 1a shows the morphology and particle size of the purchased Bi_2O_3-1. It can be seen that the Bi_2O_3 is spherical and uniformly dispersed. Its average particle size is 170 nm. Figure 1b shows Bi_2O_3-2 synthesized by hydrothermal calcination method, and its morphology is strip. Under high pressure and high temperature environment, the formed particles have regular shape, smooth surface. The agglomeration phenomenon between particles is not obvious. The dispersion is good. After measurement and calculation, the average particle size of Bi_2O_3-2 is 370 nm. The particle size and morphology information of Bi_2O_3 are shown in Table 1.

It can be seen from Figure 1c that the morphology of Bi_2O_3-3 synthesized by precipitation calcination method is coral like. Due to the high-speed magnetic stirring during water bath heating, the citric acid solution added is dispersed into small droplets, which helps to disperse the particles to a certain extent. After measurement and calculation, the average particle size of Bi_2O_3-3 is 740 nm.

In Figure 2, the synthesized Bi_2O_3 is detected by XRD and its phase is analyzed.

As can be seen from Figure 2, the Bi_2O_3-1 and Bi_2O_3-2 and Bi_2O_3-3 synthesized by (MDI jade 6.0) matching are monoclinic Bi_2O_3 phases. The lattice constants are $a=5.8486$ Å, $b=8.1648$ Å, $c=7.510$ Å, $\alpha=90.0°$, $\beta=112.977°$ and $\gamma=90.0°$. Compared with the standard spectrum of Bi_2O_3, no obvious impurity peak is found in the XRD spectrum, indicating that the purity of Bi_2O_3 is high.

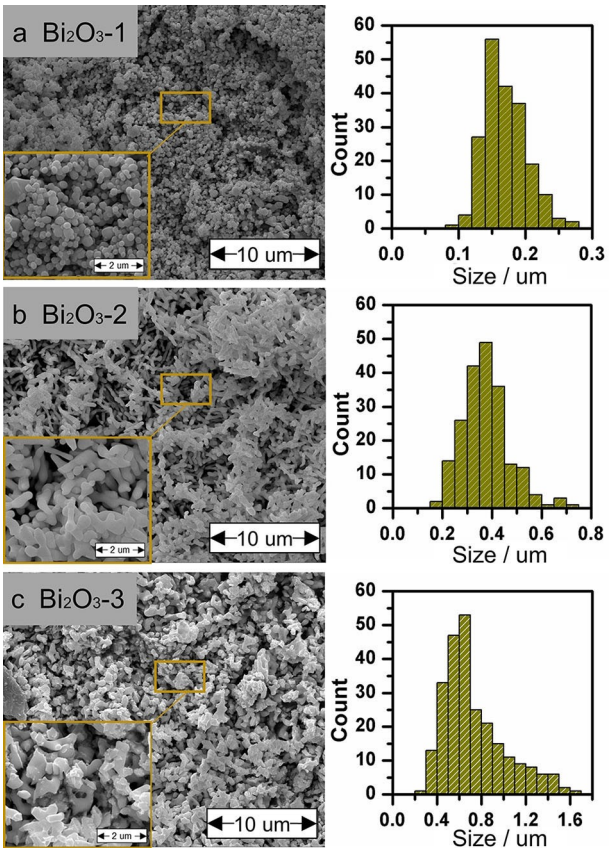

Figure 1. SEM and particle size distribution of Bi_2O_3.

2.2. Analysis on the Dispersion of Thermite

Figure 3 shows the distribution of Bi_2O_3 and nano-Al powder after ultrasonic dispersion and mixing. It can be seen from the figure that Al powder is evenly distributed on the surface of Bi_2O_3. In Figure 3a, the larger spherical particles are Bi_2O_3 particles, and the smaller spherical particles are nano Al powder, which are in close contact with each other. In Figure 3b, the spherical nano Al powder adheres to the surface of strip-shaped Bi_2O_3 particles, but there are more gaps due to the increase of the particle size of Bi_2O_3 particles. In Figure 3c, the particle size comparison between Al powder and Bi_2O_3 is very obvious. The surface area that can effectively contact with Al powder is greatly reduced.

2.3. Analysis of Thermal Excitation and Exothermic Performance

Thermal analysis experiments can observe the excitation temperature and heat release of the thermite system under linear heating conditions. The DSC curves of the samples were measured at a linear heating rate of 15 °C min^{-1}. The critical reaction temperature of thermite under the action of heat flux is an important index to study its reaction activity.[27]

Figure 4a is the thermal analysis result of Al-Bi_2O_3-1 thermite. Two obvious exothermic peaks appear during the whole heating process. In the temperature range of 564.52 °C–630.36 °C, the first obvious exothermic peak appeared in the DSC curve, with a peak temperature of 589.98 °C. At this stage,

Table 1. Comparison table of Bi_2O_3 morphology and particle.

Sample	Crystal form	Average particle size	Topography
Bi_2O_3-1	Monoclinic	170 nm	globular
Bi_2O_3-2	Monoclinic	370 nm	strip
Bi_2O_3-3	Monoclinic	740 nm	square

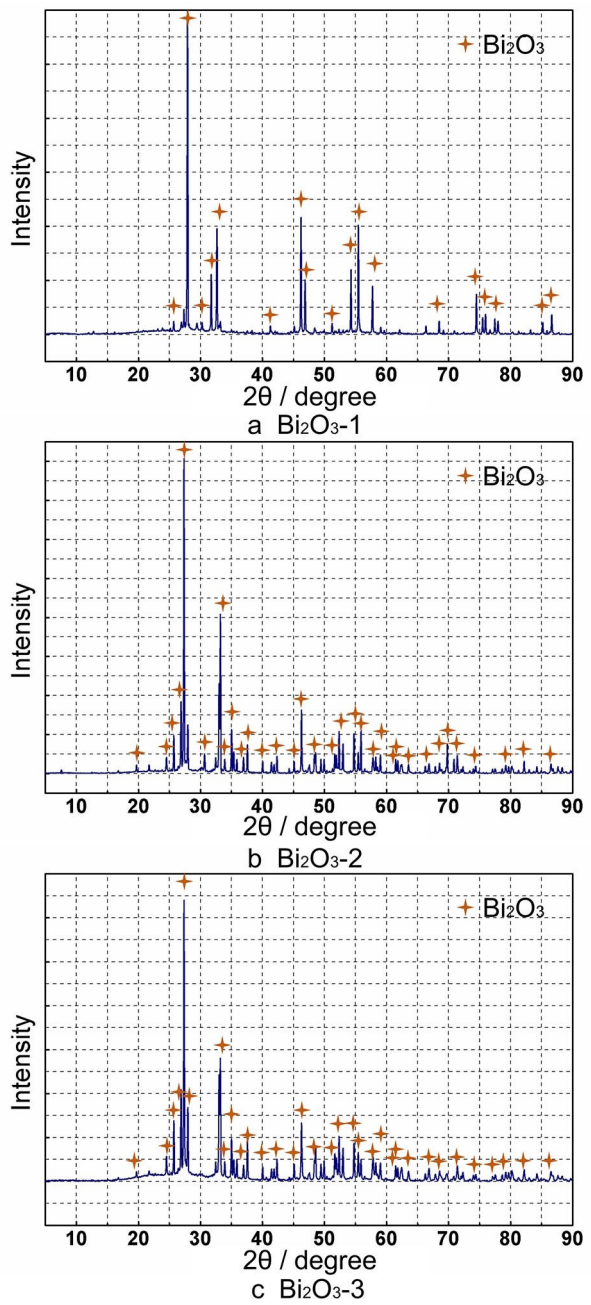

Figure 2. XRD characterization of Bi_2O_3.

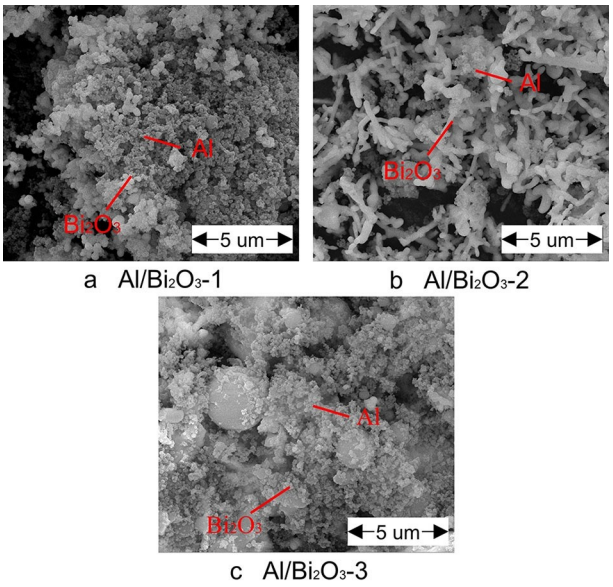

Figure 3. SEM and particle size distribution of Bi_2O_3.

both Al and Bi_2O_3 are in solid state, so the solid-solid (s-s) aluminothermic reaction occurs, and the heat release is 610.1 $J\,g^{-1}$. In the temperature range of 647.63 °C–729.64 °C, a second exothermic peak appears in the DSC curve. The melting point of Al is about 660 °C, so the melting of Al occurs in the second exothermic stage. Since the exothermic heat of the thermite reaction is much higher than the melting endothermic heat of Al, the DSC curve does not show an obvious heat absorption peak. In the second exothermic stage, Al transforms from solid to liquid, Bi_2O_3 is still solid, the thermite reaction transitions from a solid-solid (s-s) reaction state to a solid-liquid (s-l) reaction state, and the exothermic heat is 441.1 $J\,g^{-1}$.

Figure 4b is the thermal analysis result of Al-Bi_2O_3-2 thermite. The excitation temperature of the first thermite reaction lags by 93.58 °C relative to that of Al-Bi_2O_3-1. It is not until 658.1 °C that a large exothermic peak appears in the DSC curve, which lasts to 714.5 °C and the peak temperature is 676.9 °C. The heat release is 527.3 $J\,g^{-1}$, which is only 50% of the heat release of Al-Bi_2O_3-1. At this stage, the Al gradually melted, causing the outer layer of Al oxide to crack, and the molten Al overflowed to obtain a larger contact area with the Bi_2O_3. A solid-liquid (s-l) thermite reaction occurs under the stimulation of high temperature. It can be seen from the Figure 4b that there is no solid-solid thermite reaction during the entire heating period. It indicates that the increase in particle size makes the excitation threshold of the solid-solid thermite reaction higher and the heat release decreases. The melting of Al powder makes up for the problem of the decrease in contact area caused by the increase in the size of Bi_2O_3.

Figure 4c is the thermal analysis result of Al-Bi_2O_3-3 thermite. A weak exothermic peak appears at 660 °C, and solid Al begins to transform into liquid Al, absorbing part of the heat. At about 730 °C, a weak endothermic peak appears, which means that part of the Bi_2O_3 has undergone a crystalline transformation from α-Bi_2O_3 to σ-Bi_2O_3, absorbing part of the heat. During the entire heating process, there is no obvious exothermic peak before 810 °C, indicating that the solid-solid (s-s) thermite reaction does not occur during the whole stage. In the temperature range of 810.9 °C–819.2 °C, a sharp exothermic peak appears in the DSC curve, with a peak temperature of 819.2 °C and an exothermic amount of 243.6 g^{-1}. Among them, the melting temperature of Bi_2O_3 is about 820 °C, and the Al has completely melted from solid to liquid. At this stage, the thermite reaction develops from liquid-solid (l-s) to liquid-liquid (l-l) state.

From the summary in the Table 2, it can be seen that as the particle size increases, the first excitation temperature threshold

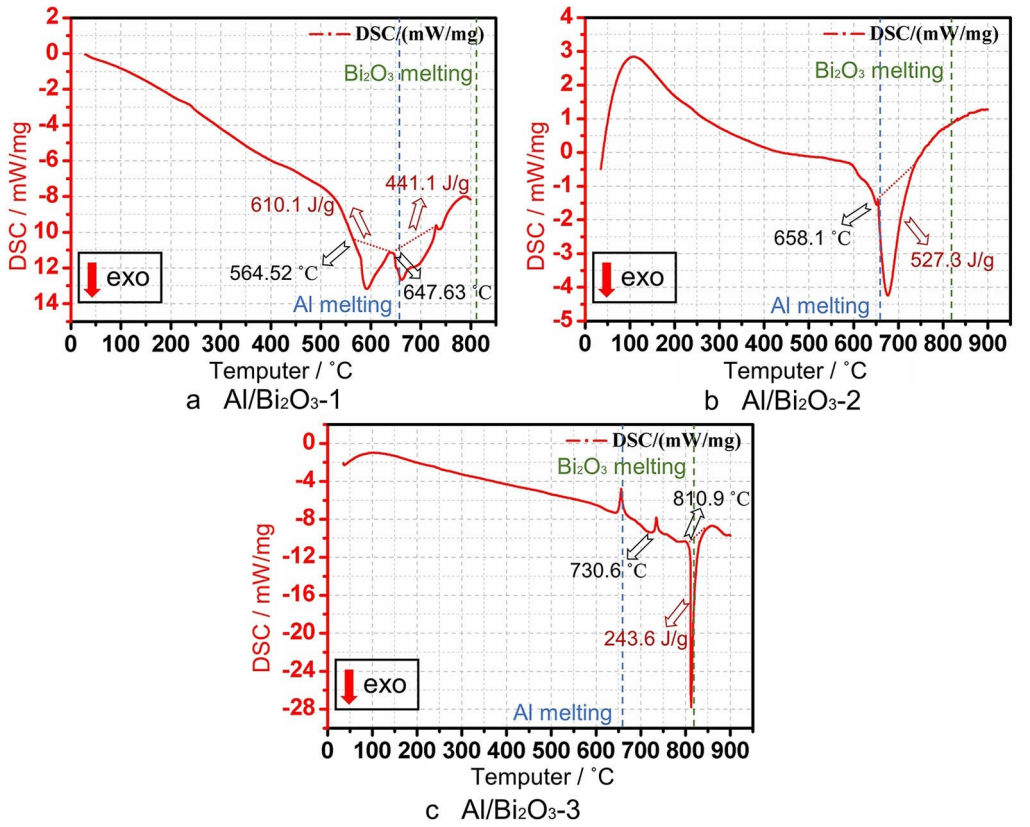

Figure 4. The DSC curves of the thermites.

Table 2. Thermite thermal analysis summary table.

Sample	T/°C	Peak 1 Q_m/ Jg^{-1}	St	Peak 2 T/°C	Q_m/ Jg^{-1}	St	Q_m/ Jg^{-1}
Al-Bi_2O_3-1	564.52	610.1	S-S	647.6	441.1	S-S/l-S	1051.2
Al-Bi_2O_3-2	658.1	527.3	l-S	–	–	–	527.3
Al-Bi_2O_3-3	810.9	243.6	l-S/l-l	–	–	–	243.6

Note: T: ignition of temperature Q: heat release St: reactant state

Table 3. Summary of excitation current.

Sample	Excitation current value/A			E(I)/A	$S^{1/2}$
Al-Bi_2O_3-1	0.503	0.541	0.640	0.561	0.0673
Al-Bi_2O_3-2	0.713	0.701	0.716	0.710	0.0290
Al-Bi_2O_3-3	0.848	0.813	0.849	0.837	0.0065

of the thermite reaction becomes higher and higher, and the heat release becomes smaller and smaller. In terms of the reaction state, the solid-solid (s-s) reaction gradually changes to the liquid-solid (l-s) reaction until the liquid-liquid (l-l) reaction changes.

The increase of the particle size of Bi_2O_3 makes the entire thermite system insensitive to external thermal excitation, causing a reduction in the number of hot spots and a reduction in the reaction rate of the reactants. This directly leads to a reduction in the amount of heat released.

2.4. Ignition and Combustion Experiments

In actual engineering applications, the performance of the thermite depends on its ignition and combustion performance. Using the onboard electric ignition device, the combustion process of a 20 mg sample to stimulate ignition was photographed, and the current value of the Ni–Cr wire flowing at the moment of ignition was recorded. As shown in Figure 6, this is a schematic diagram of an electrically activated ignition device.

From the electric ignition experiment, the thermal excitation threshold and combustion of the thermite under rapid heating conditions can be observed.

As shown in Table 3, the average excitation current values of Al-Bi_2O_3-1, Al-Bi_2O_3-2 and Al-Bi_2O_3-3 are 0.561A, 0.710A and 0.837A respectively. The standard deviations are all less than 0.1, so the excitation current measured is effective.

As shown in Figure 5, the high-speed camera captures the whole process of the combustion of three thermite samples. The current value passing through the nickel-chromium wire is used as the thermal excitation threshold of the sample under rapid heating conditions. The first picture taken after the sample is excited and ignited is 0 ms.

When the average particle size of Bi_2O_3 increases to 370 nm, as shown in Figure 5b, the excitation current value of the thermite increases to 0.716 A. The combustion duration increases to 2.5 ms, but the flame spread rate is significantly

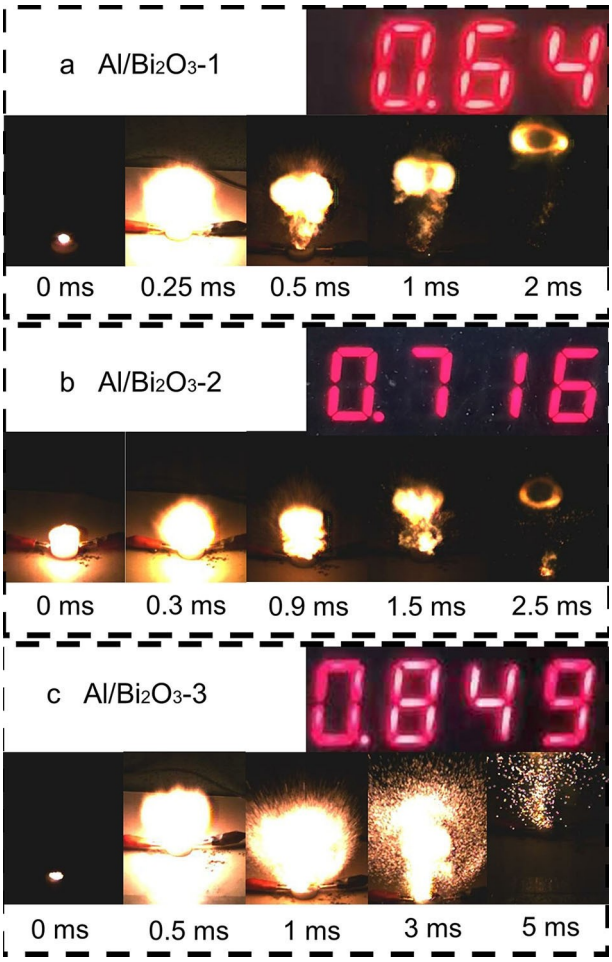

Figure 5. Electric ignition combustion diagram.

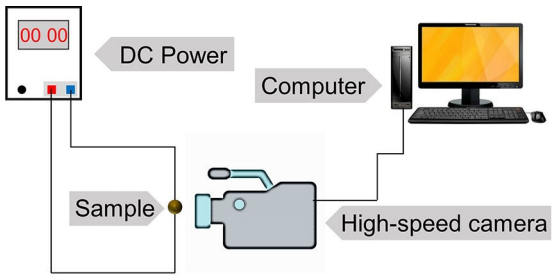

Figure 6. Schematic diagram of electric ignition excitation device.

lower than Al-Bi_2O_3-1. The increase of the particle size of Bi_2O_3 reduces the electrical conductivity of the entire thermite system.[15] At the same time that reduces the amount of drug adhered to the Ni–Cr wire per unit length, resulting in a waste of electricity.

Interestingly, in Figure 5c, when the particle size of Bi_2O_3 in the thermite system is 740 nm, the excitation current value is 0.849 A, which is not significantly increased compared to Al-Bi_2O_3-2. But there is a completely different burning phenomenon. First, the duration of its flame combustion has been increased to 5 ms, which has doubled. Secondly, different from the regular combustion properties of samples A and B, sample C was spattered by sparks and burned violently, resulting in violent sputtering.

As the particle size of the Bi_2O_3 in the thermite system decreases, the excitation current value decreases and the combustion rate increases. On the one hand, the conductivity of thermite with a smaller Bi_2O_3 particle size is lower. The contact with nickel-chromium wire is closer. This results in more thermite adhered per unit length, and higher utilization rate of the excitation energy transferred by the nickel-chromium wire. On the other hand, the reduction of the particle size of Bi_2O_3 reduces the energy barrier required for the thermite reaction to occur. This means that a larger current is required to bring a higher temperature to excite large-particle thermite samples. From an experimental point of view, in the submicron range, smaller particle sizes require lower current values under conditions of rapid heating. At the same time this also brings a higher burning rate. Therefore, it is suitable for use as an explosive,[24] but it is not conducive to the continuous progress of the reaction. A larger particle size is beneficial to enhance electrostatic safety and prolong the duration of the reaction. This is more advantageous in engineering applications such as actual welding.[9]

3. Conclusions

Three groups of thermite samples of Al(100 nm)/Bi_2O_3(170 nm, 370 nm, 740 nm) were prepared by hydrothermal synthesis and ultrasonic dispersion. Comparative study on the influence of Bi_2O_3 particle size on the thermal excitation threshold, heat release and combustion performance of the thermite system at the sub-micron scale. After research, the following conclusions were obtained:

(1) The purity of Bi_2O_3 synthesized by hydrothermal is higher. The morphology is regular and the particle size distribution is uniform. In the sample after ultrasonic dispersion, the Al powder is uniformly attached to the Bi_2O_3, and the assembly effect is better;

(2) The DSC thermal analysis experiment investigated the thermal excitation threshold and heat release of the thermite under a linear heating condition of 15 °C min^{-1}. It is found that the exothermic heat of the thermite system decreases with the increase of the Bi_2O_3 particle size, which are 1051.2 J g^{-1}, 527.3 J g^{-1} and 243.6 J g^{-1}, respectively. The thermal excitation threshold increases with the increase of the Bi_2O_3 particle size, from 564.52 °C to 810.9 °C. Through the analysis of the state of the reactants, it is found that the three kinds of Bi_2O_3 particle sizes participate in the composition of the thermite system. The first exothermic reactions are solid-solid (s-s) thermite, solid-liquid (s-l) thermite and liquid-liquid (l-l) thermite reactions.

(3) The electric ignition experiment studied the thermal excitation threshold and combustion conditions of the thermite under rapid heating conditions. The average excitation current of three groups of Bi_2O_3 is 0.561A, 0.710A and 0.837A, respectively. The combustion duration was 2 ms, 2.5 ms and 5 ms, respectively. So, the reduction of the Bi_2O_3 particle size

can significantly reduce the excitation current value of the thermite system, and increase the flame spread rate and gas production during combustion. The smaller particle size (170 nm) brings more heat sensitivity and burning speed, but it is not conducive to the continuous progress of the reaction. The larger particle size (740 nm) involved in the composition of the thermite shows the longest burning phenomenon, which is more advantageous in practical engineering applications.

Experimental Section

Materials

All chemicals are analytical reagent grade and can be used without further treatment or purification. Among them, nano-Al powder (about 100 nm) and nano-Bi_2O_3 (about 100 nm) are purchased from Aladdin Industrial Co., Ltd. (Shanghai, China). The purities are all more than 99.9%. Sodium hydroxide (NaOH), citric acid ($C_6H_8O_7$), oxalic acid /$H_2C_2O_4$) and bismuth nitrate pentahydrate (Bi-$(NO_3)_3\cdot 5H_2O$) are used to prepare Bi_2O_3 samples. They are all bought from Sichuan Kelong Company (Sichuan, China). The purities are all more than 99.5%. As for solvents and dispersant, ethyl alcohol(> 99%)and deionized water are supplied by Nanjing Chemical Reagent Co., LTD (Nanjing, China).

Hydrothermal Synthesis of Bi_2O_3

(1). Bi_2O_3 with particle size of about 170 nm was purchased from Aladdin company. The morphology is spherical. The crystal form is monoclinic. It was recorded as Bi_2O_3-1.

(2). Bi_2O_3 particles were prepared by hydrothermal method.[28] The preparation process consists of two stages of chemical reaction:

$$2Bi(NO_3)_3 + 3H_2C_2O_4 = Bi_2(C_2O_4)_3 + 6HNO_3 \quad (1)$$

$$2Bi_2(C_2O_4)_3 + 3O_2 = 2Bi_2O_3 + 12CO_2 \quad (2)$$

The detailed process is as followed: 1.26 g of oxalic acid dihydrate was dissolved in 50 ml deionized water, and 0.8 g NaOH was weighed and dissolved in oxalic acid solution. 2.91 g Bi $(NO_3)_3\cdot 5H_2O$ was placed in a beaker containing 2 ml 0.01 mol/L dilute HNO_3 and stirred until the solid was completely dissolved. The two parts of the solution were poured into a 170 ml autoclave and hydrothermally treated at 180 °C for 12 h. Subsequently, the product was centrifuged, washed, dried, and calcined at 420 °C for 4 h to obtain a light-yellow powder. It was recorded as Bi_2O_3-2.

(3). Bi_2O_3 particles were synthesized by water bath precipitation-calcination method.[29,30] The preparation process consists of two stages:

$$Bi(NO_3)_3 + C_6H_8O_7 = C_6H_5BiO_7 + 3HNO_3 \quad (3)$$

$$2C_6H_5BiO_7 + 9O_2 = Bi_2O_3 + 12CO_2 + 5H_2O \quad (4)$$

The detailed process is as followed: 2.91 g of Bi $(NO_3)_3\cdot 5H_2O$ was weighed and placed in a beaker. 5 ml of 0.01 mol/L dilute HNO_3 was added in the beaker, then ultrasonic dispersion was carried out to inhibit the hydrolysis of $Bi(NO_3)_3\cdot 5H_2O$. After that, deionized water was added to 50 ml, which was called solution A. 1.92 g of citric acid ($C_6H_8O_7$) was dissolved in 50 ml of deionized water, labeled as solution B. The beaker containing solution A was placed in a heat collecting magnetic stirring water bath pot. The bath temperature was set at 80 °C and the rotational speed was set at 60 r/s. Then, the solution B was added into solution A slowly. The solid-liquid mixture was centrifuged, washed and dried to obtain bismuth citrate ($C_6H_5BiO_7$) precursor. After being transferred to muffle furnace and calcined at 440 °C for 12 h, the light-yellow powder can be obtained. It was recorded as Bi_2O_3-3.

Characterization Method

The morphology and particle size of the samples were observed by FE-SEM (Hitachi High Technologies Corporation, s-4800 II Japan). The amplification ratio was set to $20\sim 8\times 10^5$, the maximum resolution was set to 1 nm, and the acceleration voltage was set as 0.5 ~ 30 kV. Based on SEM images, the particle size of samples was analyzed by ImageJ.

The purity of Bi_2O_3 synthesized by hydrothermal method was analyzed by XRD (Bruker, D8 advance, Germany). In the test, the Cu target was used, the goniometer radius was adjusted to $\geq$ 200 mm, and the angle range was set to 360°.

The instrument (Netzsch sta449f3, Germany) was used for DSC analysis. 3 mg of the test sample was placed in a corundum crucible. The detection whose temperature range was 25 °C to 900 °C was carried out in argon atmosphere at a heating rate of 15 °C min^{-1}.

The ignition experimental device as shown in Figure 1 was equipped to study and explore the combustion characteristics of thermite samples. The DC power was adjusted to get different values of output voltage and directly load it on a Ni–Cr wire to ignite 20 mg of samples. The diameter of Ni–Cr wire is 0.1 mm and the length is 4 cm. The frame rate of the high-speed camera (FASTCAMSA-Z, Japan) was set to 10000 fps. The whole combustion process was photographed, and the current value in the Ni–Cr wire at the moment of ignition was recorded.

Acknowledgements

This work was supported by the National Natural Science Foundation, project no.51704302. It was performed using the School of Chemical Engineering equipment at Nanjing University of Science and Technology(NUST).

Conflict of Interest

The authors declare no conflict of interest.

Keywords: combustion properties · excitation current value · heat release · particles size · thermal excitation threshold

[1] C. Rossi, *Al-Based Energetic Nanomaterials* **2016**, *2*, 1–111.
[2] A. van der Heijden, *Chem. Eng. J.* **2018**, *350*, 939–948.
[3] W. H. P. J. Liu, G. Q. He, M. Gozin, Q. L. Yan, *Adv. Mater.* **2018**, *30*,1706293.
[4] X. Zhou, M. Torabi, J. Lu, R. Q. Shen, K. L. Zhang, *ACS Appl. Mater. Interfaces.* **2014**, *6*, 3058–3074.
[5] F. Yang, X. L. Kang, J. S. Luo, Z. Yi, Y. J. Tang, *Sci. Rep.* **2017**, *7*, 9.

[6] T. An, F. Q. Zhao, Q. Pei, L. B. Xiao, X. L. Xing, H. X. Gao, X. L. Xing, *Chin. J. Inorg. Chem.* **2011**, *29*, 24–30.
[7] E. L. Dreizin, *Prog. Energy Combust. Sci.* **2008**, *35*, 141–167.
[8] V. K. Patela, R. Kantb, A. Choudharya, M. Painulya, S. Bhattacharyab, *Def. Technol.* **2019**, *15*, 98–105.
[9] B. Mihai, C. M. Ovidiu, C. T. Adrian, V. Ovidiu, *Solid State Phenom.* **2016**, *254*, 83–90.
[10] E. B. Motlagh, J. V. Khaki, M. H. Sabzevar, *Mater. Chem. Phys.* **2012**, *133*, 757–763.
[11] G. Xin, L. Jianmin, *Chemical Propellants & Polymeric Materials.* **2012**, *10*, 75–78.
[12] K. S. Martirosyan, *J. Mater. Chem.* **2011**, *21*, 9400–9405.
[13] J. K. Deng, G. P. Li, L. H. Shen, Y. J. Luo, *Bull. Chem. React. Eng. Catal.* **2016**, *11*, 109–114.
[14] T. An, F. Q. Zhao, L. B. Xiao, *Chinese Journal of Explosives & Propellants.* **2010**, *33*, 55–62.
[15] C. Weir, M. L. Pantoya, M. A. Daniels, *Combust. Flame.* **2013**, *160*, 2279–2281.
[16] L. Wang, D. Luss, K. S. Martirosyan, *J. Appl. Phys.* **2011**, *110*, 141–286.
[17] S. B. Kim, K. J. Kim, M. H. Cho, J. H. Kim, K. T. Kim, S. H. Kim, *ACS Appl. Mater. Interfaces.* **2016**, *8*, 9405–9412.
[18] K. T. Sullivan, J. D. Kuntz, A. E. Gash, *Propellants Explos. Pyrotech.* **2014**, *39*, 407–415.
[19] M. R. Weismillera, J. Y. Malchia, J. G. Leea, R. A. Yettera, T. J. Foley, *Proc. Combust. Inst.* **2011**, *33*, 1989–1996.
[20] G. C. Egan, K. T. Sullivan, T. Y. Olson, T. Y. J. Han, M. A. Worsley, M. R. Zachariah, *J. Phys. Chem. C.* **2016**, *120*, 29023–29029.
[21] S. G. Hosseini, A. Sheikhpour, M. H. Keshavarz, S. Tavangar, *Thermochim. Acta.* **2016**, *626*, 1–8.
[22] J. X. Song, T. Guo, M. Yao, J. L. Chen, W. Ding, F. L. Bei, Y. M. Mao, Z. S. Yu, J. Y. Huang, X. N. Zhang, Q. Yin, S. Wang, *Vacuum* **2020**, *176*, 109339.
[23] J. A. Puszynski, C. J. Bulian, J. J. Swiatkiewicz, *J. Propul. Power.* **2007**, *23*, 698–706.
[24] Z. X. Yi, Y. Q. Cao, J. W. Yuan, C. Mary, Z. Y. Wan, Y. Li, C. G. Zhu, L. Zhang, S. G. Zhu, *Chem. Eng. J.* **2020**, *389*, 124254.
[25] W. L. Hong, Y. F. Xue, F. Q. Zhao, J. H. Liu, H. B. Shi, S. Y. Xu, J. H. Yi, H. X. Hong, *Chinese Journal of Explosives and Propellants.* **2012**, *35*, 7–11.
[26] V. E. Sanders, B. W. Asay, T. J. Foley, B. C. Tappan, A. N. Pacheco, S. F. Son, *J. Propul. Power* **2007**, *23*, 707–714.
[27] I. Monk, M. Schoenitz, E. L. Dreizin, *Combust. Sci. Technol.* **2018**, *190*, 203–221.
[28] R. Chen, Z. R. Shen, H. Wang, H. J. Zhou, Y. P. Liu, D. T. Ding, T. H. Chen, *J. Alloys Compd.* **2011**, *509*, 2588–2596.
[29] S. Swaminathan, M. J. F. Jabeen, C. V. Niveditha, *RSC Adv.* **2015**, *5*, 78299.
[30] H. F. Cheng, B. B. Huang, J. B. Lu, Z. Y. Wang, B. Xu, X. Y. Qin, X. Y. Zhang, Y. Dai, *Phys. Chem. Chem. Phys.* **2010**, *12*, 15468–15475.

Manuscript received: December 21, 2020
Revised manuscript received: February 6, 2021